J Incl Phenom Macrocycl Chem (2012) 74:425–436
DOI 10.1007/s10847-012-0138-4

ORIGINAL ARTICLE

Ternary complexes of neodymium(III) and samarium(III) picrate triethylene glycol: structural, spectroscopic, and photoluminescent properties

Eny Kusrini · Muhammad I. Saleh · Rohana Adnan · Hoong K. Fun · M. A. Adhha Abdullah

Received: 13 January 2012 / Accepted: 1 March 2012 / Published online: 15 March 2012

Abstract The ternary complexation of neodymium(III) and samarium(III) with triethylene glycol (EO3) and picrate anion (Pic) were characterized by elemental analyses, FTIR (Fourier-transform infrared) spectroscopy, single crystal X-ray diffraction, and photoluminescence (PL). Both the $[Nd(Pic)(H_2O)_2(NO_3)(EO3)](Pic)$ and $[Sm(Pic)(H_2O)_2(NO_3)(EO3)](Pic)\cdot H_2O$ complexes were isostructural with a ten-coordination number. In both complexes, the picrate and nitrate anions were coordinated to Ln(III) in a bidentate manner, and with the the EO3 ligand in a tetradentate manner, the addition of two water molecules maintained a ten-coordination number. The lighter lanthanide-picrate complexes formed a ten-coordination number due to the lanthanide contraction effect, acyclic polyether chain length, and number of donor oxygen atoms. The acyclic EO3 ligand affected photoluminescent intensity and its conformation on the structure of the $[Ln(Pic)(NO_3)(H_2O)_2(EO3)]^+$ moiety. Photoluminescent measurement showed complex Nd(III) emissions at 403, 486, and 682 nm, with the strongest emission peak at 403 nm. Formation of these peaks occurred due to the intraligand π–π transitions of the Pic anion. The Sm(III) complex exhibited the emission characteristic of the Sm(III) ion in the red spectral region at 616.7 nm ($^4G_{5/2} \rightarrow {}^6H_{9/2}$ transition), even though the ligand emissions were also observed in the PL spectrum. The emission intensity of the 4f–4f transitions in the Sm complex was significantly higher than that found in its salt. We noted that the $[Sm(Pic)(H_2O)_2(NO_3)(EO3)](Pic)\cdot H_2O$ complex was an excellent red-light-emitter and would be considered as a candidate material for organic light emitting diodes.

Keywords Crystal structure · Neodymium complex · Photoluminescent · Samarium complex · Ternary lanthanide complexes

E. Kusrini (✉)
Department of Chemical Engineering, Faculty of Engineering, Universitas Indonesia, Kampus Baru UI, 16424 Depok, Indonesia
e-mail: ekusrini@che.ui.ac.id

M. I. Saleh · R. Adnan
School of Chemical Sciences, Universiti Sains Malaysia, 11800 Penang, Malaysia

H. K. Fun
School of Physics, Universiti Sains Malaysia, 11800 Minden, Penang, Malaysia

M. A. Adhha Abdullah
Department of Chemical Sciences, Faculty of Science and Technology, Universiti Malaysia Terengganu, 21030 Kuala Terengganu, Terengganu Darul Iman, Malaysia

Introduction

The lanthanide complexes with high and variable coordination numbers, flexible coordination environments, and luminescent properties are of interest to researchers because of their potential contributions for innovations in crystallography and the use of sensors. Luminescent lanthanide complexes are often applied as biolabels or sensors in biomedical and drug delivery applications [1, 2], primarily on the basis of their Stokes shifts, narrow emissions, and monochromatic and long-life emissions [3, 4]. The design of lanthanide complexes with strong luminescence and high stability has become a challenge in the field of emission materials. Emission quantum yields of the lanthanide complex are attributed to the balance between absorption, non-radiative decay, energy transfer, and emission rates [4–6]. The organic ligand, via its triplet

state, can absorb light and transfer energy to the Ln(III) ion.

The ability of the triethylene glycol (EO3) ligand to satisfy the coordination requirements of Ln(III) center with a high coordination number is an important criterion in the design of an emitter center for applications associated with organic light emitting diodes (OLEDs). However, the acyclic EO3 ligand also contains two terminal alcohol groups that may efficiently quench the lanthanide luminescence. Few investigations have been conducted on the structural properties of the lanthanide-triethylene glycol complexes with counter anions of halogen, NO_3^-, ClO_4^- and SCN^- [7–10]. These complexes showed the formation of salt-type compounds. A general molecular formula of $[Ln(EO3)_n(H_2O)_mX_a]\cdot X_b$, where $n = 1$–3, $m = 1$–6, $a = 1$–2, $b = 1$–3, and X = halogen, NO_3^-, ClO_4^-, or SCN^- depending on the lanthanide ion and the anion, have been previously studied [7–10].

Investigation on the effects of the acyclic short chain length of the EO3 ligand, the bulky picrate anion, and steric hindrance in the crystal structure, as well as spectroscopic, thermal, and photoluminescent properties of the lanthanide(III)-picrate complexes have been recently reported from our laboratory [11–17]. The series of EO3-Ln-Pic complexes with Ln = La, Ce, Pr, Eu, Gd, and Tb show ten- and nine-coordination numbers and exhibit high stability. Besides these structural features, coordinating water molecules incorporated in the crystal structure (except for the La complex) have been reported [11–17]. For this study, the phenomena and behavior of lighter lanthanide complexes with triethylene glycol in the presence of picrate anions was of particular interest to the authors.

As a part of our series of studies on lanthanide-picrate-EO3 complexes, new neodymium(III) and samarium(III) complexes, $[Nd(Pic)(H_2O)_2(NO_3)(EO3)](Pic)$ and $[Sm(Pic)(H_2O)_2(NO_3)(EO3)](Pic)\cdot H_2O$, were synthesized. The present work explores the crystal structures, as well as spectroscopic, and photoluminescent properties of the Nd(III) and Sm(III) complexes by using elemental analyses, FTIR, single crystal X-ray diffraction, and photoluminescence. Potential contributions of these studies include the design and syntheses of the crystal structures of lighter lanthanide complexes in the presence of bulky picrate anions with a short chain length of the acyclic EO3 ligand. We investigated the effects of picrate anions containing nitro withdrawing groups and a short chain length of acyclic ligand on photoluminescent properties and examined the energy transfer process from the acyclic or aromatic ligands to the Ln(III) ion for enhancing photoluminescent intensity.

Experimental

Materials

Triethylene glycol [$C_6H_{14}O_4$, 99 %] was purchased from Acros (New Jersey, USA); picric acid [$(NO_2)_3C_6H_2OH$, >98 %] was purchased from BDH (Poole, England). The $Sm(NO_3)_3\cdot 6H_2O$ and $Nd(NO_3)_3\cdot 6H_2O$ salts (99.9 % grade) were purchased from Johnson Matthey Electronics (New Jersey, USA) and Aldrich Chemical Company, Inc. (Milwaukee, USA), respectively. Other chemicals were of at least analar grade and were used without further purification.

Physical measurements

Elemental analyses were performed with a Perkin-Elmer 2400II elemental analyzer. IR spectrum was recorded on a Perkin-Elmer 2000 FTIR spectrophotometer in the region of 4,000–400 cm^{-1} by using the KBr pellets for the solid sample. A thin layer of the liquid sample (i.e. EO3 ligand) was applied to the surface of KRS-5 (thallium bromoiodide). Photoluminescent (PL) measurement was performed at room temperature with a Jobin–Yvon HR800UV system, and the data were collected and processed using Labspec Version 4 software. A HeCd laser was used for excitation at 325 nm, and the emission spectra were scanned from 330 to 1,000 nm. The PL spectra of free EO3, HPic, and their complexes were obtained when excited by absorption at 325 nm.

X-ray crystallography analyses

X-ray diffraction data was collected from a single crystal using a Bruker APEX2 CCD diffractometer with a graphite monochromatic Mo-K_α radiation at a detector distance of 5 cm with APEX2 software [18]. The collected data were reduced using the SAINT program; empirical absorption corrections were performed with the SADABS program [18]. The crystal structure was solved by direct methods and refined by least squares using the SHELXTL software package [19]. All non-hydrogen atoms were refined anisotropically; the hydrogen atoms in the carbon atoms were added from theory calculation and the hydrogen atoms in the oxygen atoms were added from Fourier maps and isotropically refined. The final refinement converged well. Data for publications were prepared with SHELXTL [19] and PLATON [20]. Crystal structure and refinement data for the compounds are summarized in Table 1. Selected bond lengths, bond angles, and torsion angles are listed in Table 2.

Table 1 Crystallography data and refinement for the Ln-(EO3-Pic) complexes

Parameter	Nd	Sm
Empirical formula	$C_{18}H_{22}N_7O_{23}Nd$	$C_{18}H_{24}N_7O_{24}Sm$
Molecular weight	848.67	872.79
Volume (Å^3)	1454.36(8)	1436.5(2)
Crystal system, space group	Triclinic, P-1	Triclinic, P-1
Z	2	2
Unit cell dimensions		
a (Å)	7.2165(2)	7.1298(6)
b (Å)	8.3750(3)	12.8028(11)
c (Å)	24.5078(7)	16.9777(14)
α (°)	95.3890(10)	71.043(4)
β (°)	90.9440(10)	78.923(4)
γ (°)	99.3380(10)	89.113(4)
Calculated density (g/cm^3)	1.938	2.018
Absorption coefficient (mm^{-1})	1.898	2.163
F(000)	846	870
Crystal size (mm)	0.50 × 0.50 × 0.22	0.25 × 0.14 × 0.08
Theta (θ) (°)	0.83–37.50	1.29–30.00
Limited index	$-12 \le h \le 12$, $-14 \le k \le 13$, $-41 \le l \le 41$	$-10 \le h \le 10$, $-18 \le k \le 18$, $-23 \le l \le 23$
Reflections collected/unique	49745/15200	35726/8346
	[R(int) = 0.0233]	[R(int) = 0.0564]
Refinement method	Full-matrix least-squares on F^2	Full-matrix least-squares on F^2
Data/restraint/parameter	15200/0/456	8346/0/459
Goodness-of-fit on F^2	1.297	1.153
Final R indices [$I>2\sigma(I)$]	$R_1 = 0.0347$, $wR_2 = 0.0754$	$R_1 = 0.0286$, $wR_2 = 0.0671$
R indices (all data)	$R_1 = 0.0375$, $wR_2 = 0.0771$	$R_1 = 0.0336$, $wR_2 = 0.0787$
Largest diff. peak and hole (e.Å^{-3})	1.650 and −3.774	1.645 and −1.266

Table 2 Selected bond length (Å), bond angle (°) and torsion angle (°) of the Ln-(EO3-Pic) complexes

Atom	Bond length (Å)		Atom	Torsion angle (°)		Atom	Bond angle (°)	
	Nd	Sm		Nd	Sm		Nd	Sm
Ln1–O1	2.506(2)	2.465(2)	O1–C1–C2–O2	53.6(3)	−54.7(3)	O1–Ln1–O2	63.1(6)	64.2(7)
Ln1–O2	2.536(2)	2.515(2)	O2–C1–C2–O3	−53.4(2)	−54.0(3)	O2–Ln1–O3	62.3(5)	63.5(6)
Ln1–O3	2.565(2)	2.525(2)	O3–C1–C2–O4	−46.0(5)	54.0(3)	O3–Ln1–O4	63.0(5)	63.6(7)
Ln1–O4	2.552(2)	2.459(2)	C2–O2–C3–C4	−165.0(2)	−173.1(2)	O4–Ln1–O1	141.2(6)	147.8(7)
Ln1–O5	2.378(1)	2.293(2)	C3–O2–C2–C1	169.6(2)	−98.7(3)	Average O–C–C	110.1(3)	106.5(2)
Ln1–O6	2.601(2)	2.909(2)	C4–O3–C5–C6	–	168.5(2)	Average C–O–C	112.1(3)	113.3(2)
Ln1–O12	2.621(2)	2.445(2)	C4–O3–C5–C6A	−122.6(4)	–			
Ln1–O14	2.613(2)	2.609(2)	C4–O3–C5–C6B	−162.3(6)	–			
Ln1–OW1	2.441(2)	2.497(2)	C5–O3–C4–C3	−176.6(3)	−173.5(2)			
Ln1–OW2	2.563(2)	2.392(2)						
Average C–O	1.438(4)	1.440(3)						
Average C–C	1.445(8)	1.503(4)						

Crystal preparation of Ln-(EO3-Pic) complexes

The Nd(III) and Sm(III) complexes were prepared utilizing a procedure similar to that which was previously described for the Ln-EO3-Pic complexes [11–17]. The EO3 ligand (0.454 g, 3.0 mmol), Pic (0.917 g, 4 mmol), and each mmol of $Ln(NO_3)_3{\cdot}nH_2O$, where Ln = Nd or Sm were added to 30 mL acetonitrile:methanol:water (3:3:1 v/v).

The mixture (solution) was filtered into a 100 mL beaker, and the resulting solution was stirred for 10 min at room temperature. The resultant yellow solution was left covered to allow slow evaporation at room temperature. After a few weeks, block-shaped crystals began to form. To obtain single crystals suitable for X-ray diffraction, the crystals were recrystallized in CH_3OH, CH_3CN, CH_3OH:CH_3CN (1:1, v/v), and CH_3OH solvents, respectively. The light brown single [Nd(Pic)$(OH_2)_2(NO_3)$(EO3)](Pic) crystal was collected by filtration from the CH_3OH solvent after 8 months with 85 % yield. The yellow single [Sm(Pic)$(OH_2)_2(NO_3)$(EO3)]$^+$(Pic)$^-\cdot H_2O$ crystal was isolated by filtration from the methanol solvent after 1 month with 75 % yield.

Anal. Calc. for [Nd(Pic)$(H_2O)_2(NO_3)$(EO3)](Pic): C, 25.48; H, 2.61; N, 11.55. Found: C, 26.27; H, 2.08; N, 11.50. Decomposition point: 131–182.1 °C. Color : Light brown (brownish). IR (ν/cm^{-1}): 3382(b), 1579(s), 1546(s), 1366(s), 1343(s), 1083(s), 1063(s), 1274(s), 1489(s), 813(w), 936(s), 788(s).

Anal. Calc. for [Sm(Pic)$(H_2O)_2(NO_3)$(EO3)](Pic)$\cdot H_2O$: C, 24.74; H, 2.75; N, 11.23. Found: C, 23.98; H, 2.40; N, 10.83. Decomposition point: 121.4–182.1 °C. Color: Yellow. IR (ν/cm^{-1}): 3367(b), 1564(s), 1560(s), 1370(s), 1334(s), 1081(s), 1269(s), 1483(s), 813(w), 937(s), 795(s).

Results and discussion

Physical properties and spectral analysis

For the neodymium complex, a distinct change from the yellow color typical of the metal picrates to a light brown was observed in solution, finally producing the brownish crystal. However, in the case of the samarium complex, no change in the color of solution could be observed by naked eye, and the yellow crystals were collected. These yellow crystals of the Sm complex could be explained by the colorless precursor Sm salt, indicating complete dependence on the color of the picrate anion. A small amount of water solvent in the mixture (solution) helped the Ln-EO3-Pic complexes to form more readily compared to the solution without water molecules. Adding a small amount of water to the solution because of the small chain length of the acyclic EO3 ligand was suggested in the literature [11, 12, 21]. The complexes were stable in air and moisture for a long period, although they contained water molecules. As noted in our previous studies for the Ln-EO3-Pic complexes, they were soluble in dimethyl sulfoxide and slightly soluble in acetone, acetonitrile, methanol, and water. However, they were insoluble in chloroform, ethyl acetate, and toluene.

The elemental analysis data of the complexes were consistent with the molecular formulae obtained from the X-ray analysis. The maximum 0.5 % mismatch for the analytical data could be understood by the fact that each complex has a heavy atom, which could affect accuracy for the lighter atoms. Chemical structures of the [Nd(Pic)$(H_2O)_2(NO_3)$(EO3)](Pic) and [Sm(Pic)$(H_2O)_2(NO_3)$(EO3)](Pic)$\cdot H_2O$ complexes were confirmed by single-crystal X-ray diffraction.

As shown in Fig. 1a, the IR spectrum of the EO3 ligand exhibited broad bands stretching from ν(O–H) at 1,115–1,070 cm^{-1} and ν(C–O) at 3,368 cm^{-1}. Both complexes had higher ν(O–H) stretching frequencies for the alcohol groups than for the free ligand; they shifted to lower frequencies in the range of 33–34 cm^{-1}, indicating chelation of the EO3 ligand with Ln(III). The band due to the ν(C–H) symmetric stretching at 2,879 cm^{-1} shifted to a higher frequency at 2,971–2,973 cm^{-1}, showing that conformation of the EO3 ligand had changed to a pseudocyclic conformation (Fig. 1b). In the OH phenolic groups, out-of-plane bending vibrations of the Pic molecule at 1,151 cm^{-1} disappeared, indicating that the hydrogen atom of the phenolic groups participated in coordination and was replaced by Ln(III). The presence of the coordinated Pic anion through its nitro groups was confirmed by strong bands at 1,579–1,564 and 1,560–1,546 cm^{-1}, and at 1,370–1,366 and 1,343–1,334 cm^{-1}. The absorption band corresponding to the OH terminal groups of the EO3 ligand at 656 cm^{-1} was not observed in either complex, indicating that both terminal alcohol groups were coordinated with the Ln(III) ion. Absorption bands at 546 and 521 cm^{-1} were definitively observed in both complexes, indicating that the Ln(III) had coordinated with the oxygen atoms of the EO3 ligand.

The absorption bands assigned to the coordinated nitrate group were observed at 1484–1489 cm^{-1} (ν1), 1327 cm^{-1} (ν4), 1024–1026 cm^{-1} (ν2), and 813 cm^{-1} (ν3). Asymmetric ν_a(N–O) and symmetric ν_s(N–O) stretching at 1,484–1,489 and 813 cm^{-1} were present due to nitrate anions in the complexes, which were indicative of bidentate chelation of a nitrate anion with Ln(III) [22–26]. In addition, the separation of the two strongest frequencies [ν1–ν4] was approximately 157–161 cm^{-1}, clearly establishing that the nitrate group in the complexes was coordinated to Ln(III) as bidentate ligands [22, 24]. The absence of absorption bands at 1380, 820, and 720 cm^{-1} in the spectra of complexes indicated that the free nitrate anion is not present in the complex.

X-ray studies

The acyclic EO3 ligand formed a cyclic structure after the ternary complex formation with the Nd(III) and Sm(III) ions. A significant structural change was found in the Nd

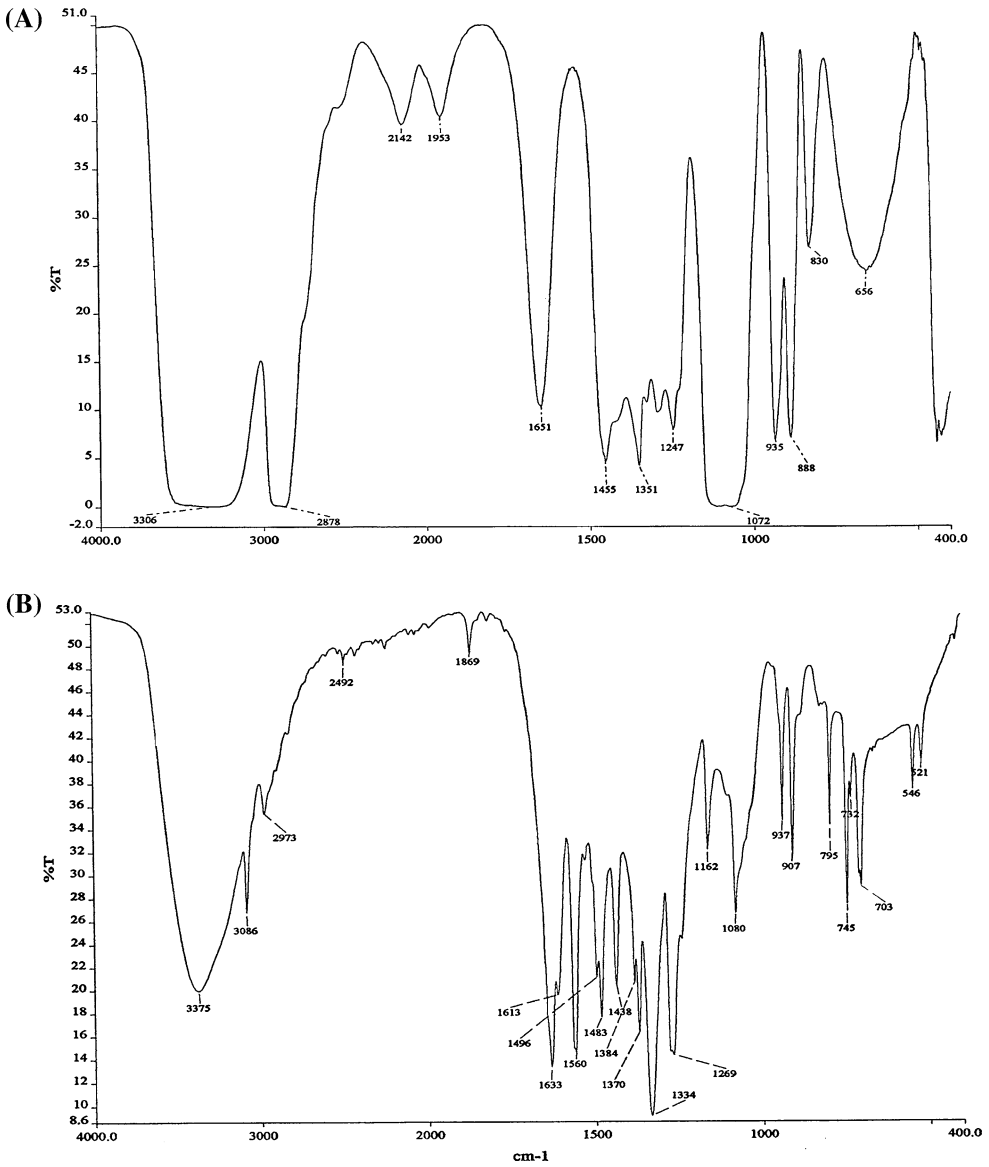

Fig. 1 Comparison FTIR spectra of the EO3 ligand (**a**) and the $[Sm(Pic)(H_2O)_2(NO_3)(EO3)](Pic)\cdot H_2O$ complex (**b**)

and Sm complexes compared to the analogs–the La, Gd, and Tb picrate complexes [11, 16, 17]. The nitrate anion had appeared in the inner-coordination sphere, replacing one picrate anion and leading to a formulation of $[Ln(Pic)(H_2O)_2(NO_3)(EO3)](Pic)$. We assumed that the nitrate anion was present in the complex because it had replaced the water molecule and/or picrate anion. Both the Nd(III) and Sm(III) complexes are isostructural with molecular formulae of $[Nd(Pic)(H_2O)_2(NO_3)(EO3)](Pic)$ and $[Sm(Pic)(H_2O)_2(NO_3)(EO3)](Pic)\cdot H_2O$, respectively (Fig. 2). These structures are similar structures to the analogs of lighter lanthanide-picrate complexes for Ln = Ce, Pr, or Eu [13–15]. The solvated water molecules was only observed in the Sm complex. Furthermore, the complexes were crystallized in triclinic systems with space group P-1. Unlike $[Ln(NO_3)_3(EO3)]$ for Ln = Pr–Dy [7, 9, 21, 26] and $[Ln(OH_2)_5(EO3)]Cl_3$ for Ln = Nd–Y [7–9], ten- and nine-coordination numbers were observed for the Nd(III) and Sm(III) complexes, respectively. In the $[Ln(NO_3)_3(EO3)]$ and $[Ln(OH_2)_5(EO3)]Cl_3$ complexes, the Ln(III) ion was coordinated to the EO3 ligand and completed with three nitrate anions; on the other hand, a counter anion was composed of three chloride anions [7–9, 21, 26]. For comparison, the [(pic-O)Sm{(L–H)(EtOH)0.5(CH2Cl2)0.5}](pic)·EtOH·2H2O complex showed a nine-coordination number, with the picrate anion acting as a monodentate chelator for the Sm(III) ion, where L = 5,11,17,23-tetra-tert-butyl-24-hydroxy-26,27,28-tris(diethylcarbamoylmethoxy)calix[4]arene [27].

As the lanthanide radii in the $[Gd(Pic)_2(H_2O)(EO3)](Pic)\cdot CH_3OH$ [16] and $[Tb(Pic)_2(H_2O)(EO3)](Pic)0.0.5(EO3)$

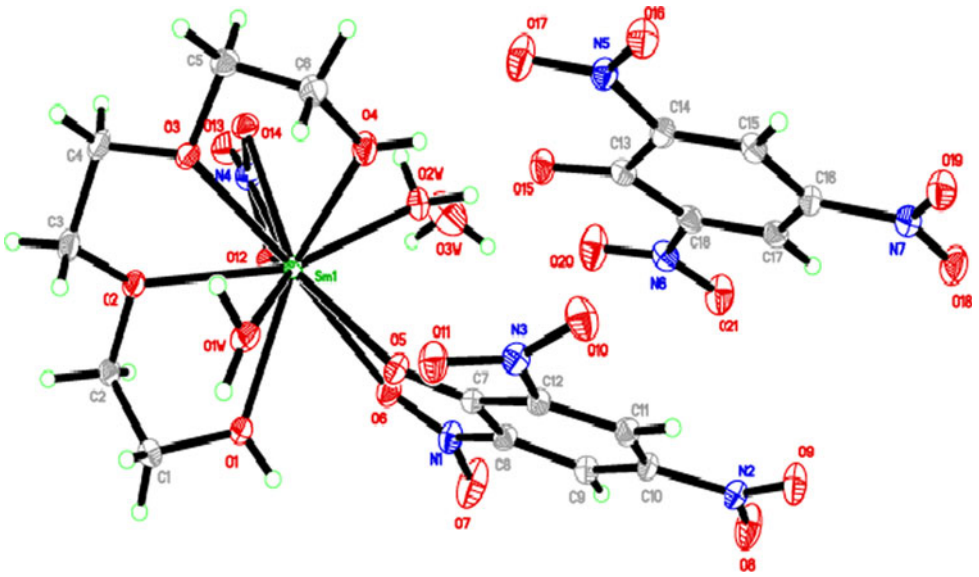

Fig. 2 Molecular structure of $[Sm(Pic)(H_2O)_2(NO_3)(EO3)](Pic)\cdot H_2O$ with atom numbering of 50 % ellipsoid probability

[17] complexes decreased, the nitrate anion could no longer be accommodated in their inner-coordination spheres. The Ln(III) metal ions displayed nine coordinates; two Pic anions, one water molecule, and one EO3 ligand had been incorporated [16, 17]. Two picrate anions appeared in the inner-coordination spheres of the heavier lanthanide complexes [16, 17]; thus, we concluded that the picrate anion played a significant role in changing the geometries and coordination environments in the complexes due to lighter or heavier lanthanides, as well as acyclic ligands. In this study, both the EO3 and Pic ligands controlled the inner-coordination spheres of the complexes; moreover, the lanthanide contraction effect also influenced the coordination numbers in each complex. We noted that the Ln(III) center can form complexes with nine or ten coordinates, depending on the size of the Ln(III) ion and anions associated with charge balancing and steric hindrance.

When we used a short length of acyclic ligand, such as EO3, we observed incorporation of water molecules with the Ln(III) ion. We also observed that the acyclic ligand was incapable of providing e oxygen donor atoms, and steric hindrance around the Ln(III) from the bulky picrate anion, EO3, and nitrate anion appeared to be a factor. These coordination bond occured because of the favorable matching between Ln(III) and the oxygen donor atom. Thus, the outer spheres of the complexes were formed and the necessary coordination number was attained, both owing to two water molecules. We noted that the lack of saturation of the inner-coordination sphere facilitates easy reactions, either with a donor solvent or with a nucleophilic impurity (i.e. water) that ultimately leads to a poorly volatile or involatile hydroxocomplex [28].

In the present study, each Ln(III) ion was coordinated to ten oxygen atoms from one EO3 ligand (O1, O2, O3, and O4), one picrate anion (O5 and O6), one nitrate anion (O12 and O14), and two water molecules (O1W and O2W), resulting in a coordination number of ten. Coordination of the Pic and NO_3 anions to Ln(III) occurred in a bidentate manner. The picrate anion was chelated to Ln(III) via an oxygen atom of the phenolic group (O5) and an oxygen atom of the *ortho*-nitro group (O6) (Fig. 3a, b). The acyclic EO3 ligand formed a ring-like structure, together with the nitrate anion situated on the same side with the EO3 chain, while the Pic anion remained at the open side of the EO3 chain. We identified the coordination polyhedrons of the Nd(III) and Sm(III) complexes as decatetrahedron and bi-capped square-antiprismatic geometries, respectively. The coordination polyhedron of the Sm(III) complex was characterized by a slightly distorted bicapped square-antiprismatic geometry with the O2 and O14 atoms at the peak of the capping position (Fig. 4).

Crystal data and structural parameters for both complexes are described in Tables 1 and 2. We noted that the Ln-O_{EO3} bond lengths decrease with a decreasing metal atom radius, as do the Ln-$O_{phenolic}$ and Ln-O_{nitro} bond lengths of the picrate anion. The Ln-O_{EO3} bond lengths between the Nd(III) ion and the oxygen atoms ranged from 2.506(2) to 2.565(2) Å, longer than those in the Sm complex (2.465(2)–2.525(2) Å). As expected, the Ln1-$O_{alcoholic}$ bond lengths were shorter than the Ln-$O_{etheric}$ bond lengths (Table 2); averages of the Ln-$O_{phenolic}$ bond lengths were the shortest. Differences were attributed to the higher electron density of the oxygen phenolic group of the picrate anion [11–17, 22, 25]. The Ln-$O_{alcoholic}$ bond lengths in the

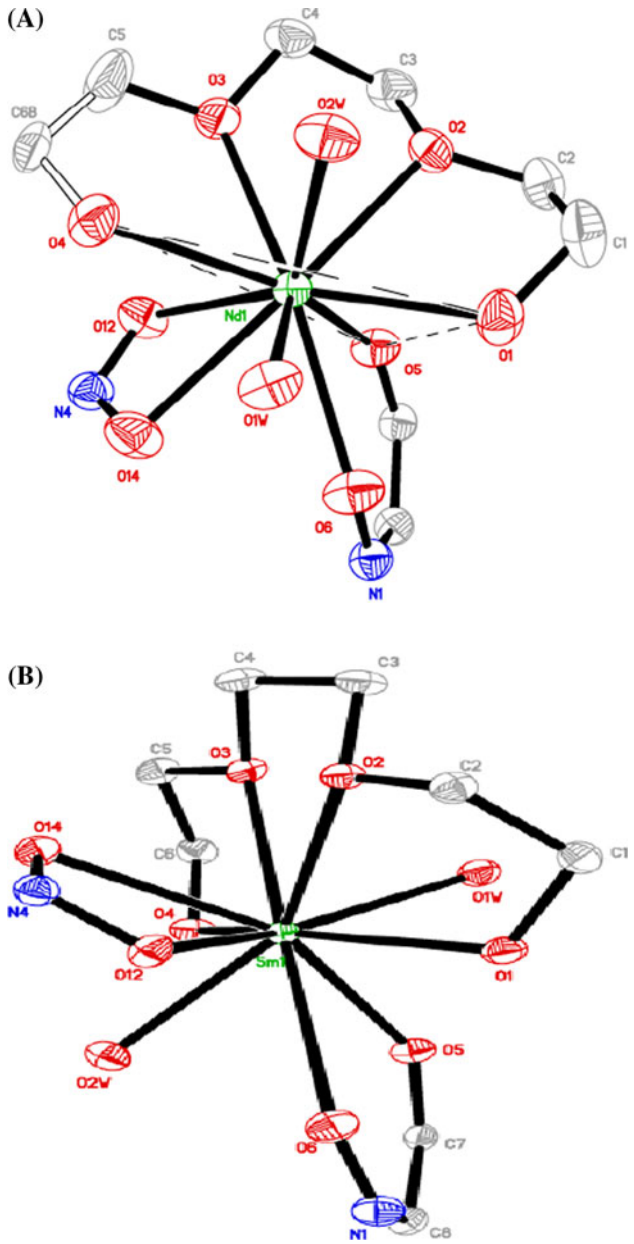

Fig. 3 The inner coordination spheres of $[Nd(Pic)(H_2O)_2(NO_3)(EO3)]^+$ (**a**) and $[Sm(Pic)(H_2O)_2(NO_3)(EO3)]^+$ (**b**)

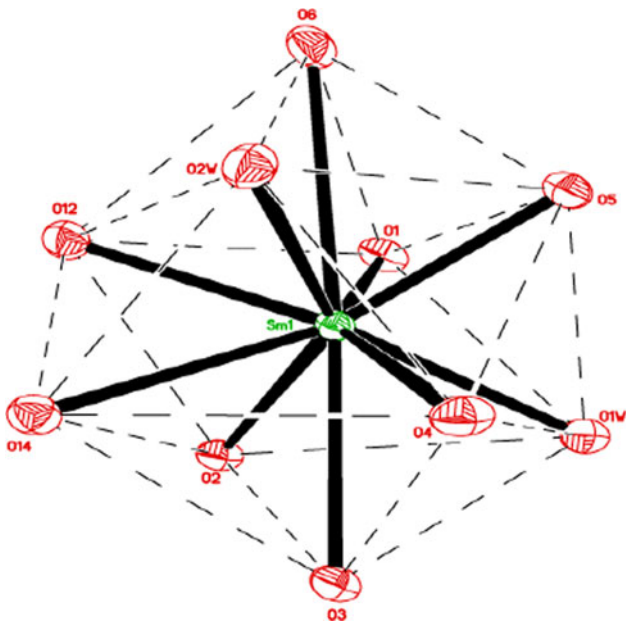

Fig. 4 Coordination geometry around the Sm(III) ion in bicapped square antiprismatic geometry

inner-coordination sphere of Ln-EO3 were 2.529(2) and 2.462(2) Å, respectively, for the Nd and Sm complexes; the Ln-$O_{etheric}$ bond lengths in the inner-coordination sphere of Ln1-EO3 were 2.551(2) and 2.520(2) Å, respectively, for the Nd and Sm complexes. However, the Ln-O_{nitro} bond length was the longest at 2.601(2), and 2.909(2) Å, respectively (Table 2). Further, the average Ln-$O_{nitrato}$ bond lengths were 2.617(2), and 2.527(2) Å, respectively, for the Nd and Sm complexes; bond length was quite similar for the $[Nd(NO_3)_3(EO3)]$ complex (2.548(3) Å) [21]. In fact, the bond lengths, and bond angles and torsion angles in the Nd and Sm complexes were quite similar as a result of the lanthanide contraction effect. The ionic radii of Nd(III) and Sm(III) were 1.163 and 1.132 Å, respectively, effectively forming a nine-coordination number [27, 29]. The C–O and C–C bond lengths of the EO3 ligand for both complexes were similar and comparable to those of the $[Ce(Pic)(H_2O)_2(NO_3)(EO3)](Pic)$ and $[Eu(Pic)(H_2O)_2(NO_3)(EO3)](Pic)0.0.73H_2O$ complexes [14, 15]. The C–O bond lengths of the EO3 ligand in Nd complex were longer than those found in the Ce complex, indicating strong coordination ability of Nd relative to Ce. The average C–$O_{phenolic}$ bond lengths of the coordinated picrato of 1.263(4) Å were slightly longer than the average C–$O_{phenolic}$ bond length of the picrate counter anion [1.253 (4) Å]; the difference was based on elongation of the Ln–O5 bond.

The chelated picrate and nitrate anions are on the same side of the inner-coordination sphere of Nd-EO3 system. This sitution is similar as observed in the Ce complex [12]. We noted that the Nd1/O1/O4/O5 was planar, with maximum deviation for atom Nd1 of 0.022(1) Å from the least-square plane (Fig. 3a). The coordinated picrate O5/C7/C8/O6 (maximum deviation 0.047(1) Å at atom O5) and nitrato O12/N4/O13/O14 (maximum deviation 0.006(3) Å at atom N4) fragments also were planar. In this study, however, the Nd1 atom deviated by 0.550(1) and 0.528(1) Å from both fragments, respectively. Both fragments were inclined toward each other by dihedral angles of 76.7(1)° for the Nd complex. The Sm1/O12/O13/O14/N4 fragments were planar with a maximum deviation of 0.019(3) Å for the O13 atom, and the Sm1/O2/O3/O4 fragments were

planar with a maximum deviation of 0.024(1) Å for the Sm1 atom. Both the coordinated picrato O5/C7/C8/O6 and nitrato O12/N4/O13/O14 fragments were inclined toward each other by dihedral angles of 54.5(1)° for the Sm complex (Fig. 3b).

The O–Ln–O bond angles between adjacent oxygen atoms in the EO3 ligand slightly exceeded 60° (Table 2). Bond angles for O1–Ln–O4 between the oxygen of terminal alcohol groups were between 141.4(1) and 147.7(1)°. Thus, the inner-coordination spheres of the complexes displayed pseudocyclic conformations (Fig. 3a, b). The O–C–C–O torsion angles from the ring of the EO3 ligand in both complexes used the conformation patterns of $g^+ g^- g^-$; and $g^- g^- g^+$, respectively. All the C–O–C–C torsion angles were *anti*, except for C3–O2–C2–C1, which closely resembled the *gauche* conformation (g^-) for the Sm complex.

Hydrogen bonding as a key factor in defining molecular packing and various intra- and intermolecular interaction was observed in both complexes. The arrangement of hydrogen bonding through an infinite one-dimensional chain by operational direction of (100) was observed in the Nd complex. In the Nd complex, the disordered C6 atom of the EO3 ligand was stabilized by intra- and intermolecular O–H···O and C–H···O hydrogen bonding involving the oxygen atoms of the coordinated picrate, water molecules, and picrate counter anion with hydrogen atoms of the picrate anion, water and EO3 ligand; subsequently, a one-dimensional network was formed (Fig. 5a; Table 3). In the Sm complex, the solvated water molecule (OW3) contributed to the formation of a weak intermolecular O3W–H23W···O21 hydrogen bond of 2.340 Å (Table 3). Two bifurcated hydrogen bonds, namely O4–H4C···O15 and O4–H4C···O17, and O2W–H12W···O15 and O2W–H12W···O20, were also observed in the Sm complex (Fig. 5b). In contrast to the Ce complexes [12], the Nd complex had face-to-face, π–π interactions between the chelated picrate anions with their centroids separated by 4.506(1) Å (symmetry code $-1-x, -y, -1-z$) (see Fig. 5a). The picrate counter anion showed alternating π–π stacking with a centroids distance of 4.007(2) Å (symmetry code $2-x, -y, -z$). Weak π–π interactions in the range of 4.007(2) to 5.398(2) Å were observed for both the Nd and Sm complexes.

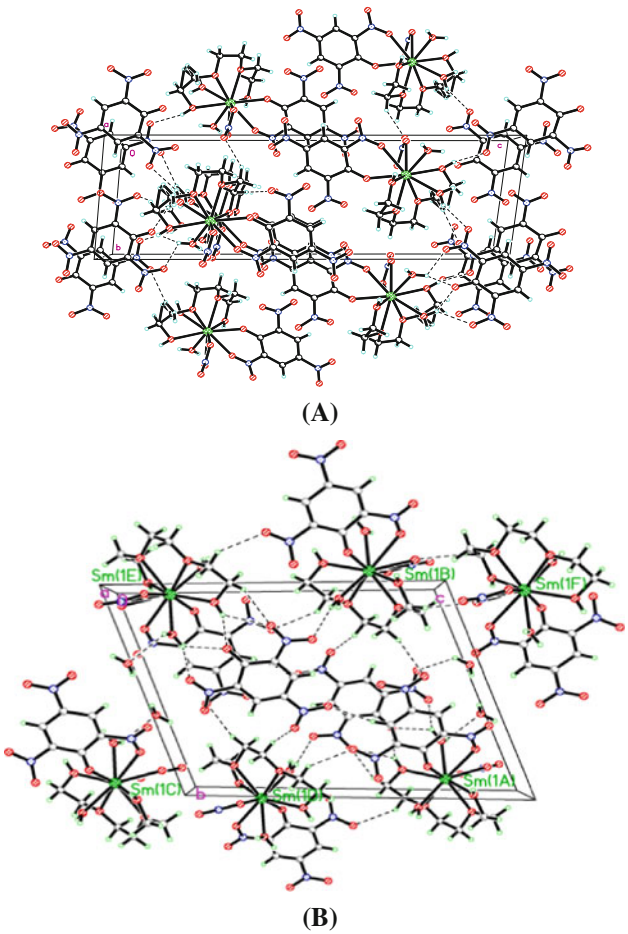

Fig. 5 Crystal packing of the $[Nd(Pic)(H_2O)_2(NO_3)(EO3)](Pic)$ (**a**) and $[Sm(Pic)(H_2O)_2(NO_3)(EO3)](Pic)\cdot H_2O$ (**b**) complexes viewed down the *a*-axis. The *dashed lines* show O–H···O and C–H···O hydrogen bonding

Photoluminescent characteristics

The $[Gd(Pic)_2(H_2O)(EO3)](Pic)\cdot CH_3OH$ complex was selected for determination of the triplet state energy of the picric acid (HPic) ligand. The phosphorescent spectra of the ternary Gd complex with the HPic and EO3 ligands and the free HPic molecule were investigated and displayed a green emission (Fig. 6a, b). The triplet state energy level of the HPic molecule [T_1(L)] was 18,622 cm^{-1}, based on the highest phosphorescent bands around 537 nm. The HPic molecule contains three nitro groups; thus, the triplet state energy of the HPic molecule was lower than that found in 5-nitro-1-10-phenantroline (20,048 nm^{-1}) [30]. The lowest excited resonance level of Sm(III), $^4G_{5/2}$ (17,900 cm^{-1}), was above the triplet state energy level of the HPic ligand. However, the lowest excited resonance level of the Nd(III) ion, $^4F_{3/2}$ (10,753 cm^{-1}), was below the ligand's triplet state energy level. We noted that T_1(L) could be transfered to the Ln(III) central metal ion if it was higher than the lowest resonance level of the Ln(III) ion. In fact, it is effectively transferred to the Ln(III) ion with energy differences of 2,500–3,500 cm^{-1} [30, 31]. Sensitization of the metal-centrered emission was observed for the Sm complex, owing to the fact that $^4G_{5/2}$ level was lower in energy ($\Delta E = 722$ cm^{-1} and the band gap energy between T_1(L) and the lowest resonance energy level of Nd(III) was too large; therefore, inefficient energy transfer and lack of a metal-centered emission resulted.

Table 3 Hydrogen bonding in the Nd(III) and Sm(III) complexes

D–H···A	D–H (Å)	H···A (Å)	D···A (Å)	D–H···A (°)
The Nd(III) complex				
O1–H1C···O12^{i}	0.8202	2.0016	2.812(2)	169.28
O4–H4C···O18^{ii}	0.8193	2.1511	2.855(3)	144.07
O1W–H11W···O15^{iii}	0.7467	1.9410	2.662(2)	162.35
O1W–H11W···O20^{iii}	0.7467	2.5396	2.962(4)	117.81′
O2W–H12W···O21^{iv}	0.7372	2.3668	3.034(3)	151.19
O1W–H21W···O13^{i}	0.8769	1.9254	2.795(3)	170.74
O2W–H22W···O15^{iii}	0.7975	2.0634	2.788(3)	151.08
O2W–H22W···O17^{iii}	0.7975	2.4859	3.105(3)	135.39′
C1–H1A···O11^{i}	0.9707	2.4388	3.409(4)	177.90
C2–H2A···O13^{v}	0.9697	2.4619	3.318(3)	147.03
C3–H3A···O11^{c}	0.9704	2.5090	3.452(3)	164.08
C3–H3B···O6^{vi}	0.9695	2.5806	3.477(3)	153.77
C5–H5B···O19^{vii}	0.9599	2.5182	3.450(5)	163.80
The Sm(III) complex				
O1–H1C···O14^{i}	0.84(6)	2.11(6)	2.949(3)	175(4)
O4–H4C···O15	0.81(5)	2.00(5)	2.753(3)	154(4)
O4–H4C···O17	0.81(5)	2.41(5)	3.025(3)	133(4)
O1W–H11W···O18^{ii}	0.850	2.513	3.266(3)	148.0
O2W–H12W···O15	0.850	2.130	2.755(3)	130.1
O2W–H12W···O20	0.850	2.163	2.900(4)	145.0
O1W–H21W···O16^{iii}	0.850	2.133	2.891(3)	148.4
O3W–H23W···O21^{iv}	0.851	2.340	2.947(4)	128.6
C1–H1B···O12^{v}	0.969	2.425	3.241(4)	141.5
C3–H3B···O8^{vi}	0.970	2.517	3.465(4)	165.6
C4–H4B···O18^{vi}	0.969	2.484	3.322(4)	144.6
C5–H5A···O10^{iii}	0.970	2.529	3.358(4)	143.4
C6–H6A···O17	0.970	2.543	3.076(4)	114.6
C11–H11A···O19^{vii}	0.929	2.447	3.368(4)	170.8
C15–H15A···O16^{c}	0.930	2.292	2.626(4)	100.5
C17–H17A···O21^{c}	0.930	2.282	2.622(4)	100.9

[a] Symmetry codes: (i) $1 + x, y, z$; (ii) $-1 + x, y, z$; (iii) $1 - x, -y, -z$; (iv) $1 - x, 1 - y, -z$; (v) $1 + x, 1 + y, z$; (vi) $x, 1 + y, z$; (vii) $-1 + x, 1 + y, z$

[b] Symmetry codes: (i) $1 + x, y, z$; (ii) $x, 1 + y, z$; (iii) $-x, -y, -1 - z$; (iv) $-x, -1 - y, -z$; (v) $-x, -y, -z$; (vi) $-1 + x, 1 + y, z$; (vii) $1 - x, -1 - y, -1 - z$

[c] Intramolecular hydrogen bonding

We compared the PL spectra of $[Nd(Pic)_2(H_2O)_6](Pic).6H_2O$ and $[Nd(Pic)(H_2O)_2(NO_3)(EO3)](Pic)$ complexes in the solid state to evaluate the function of the acyclic EO3 ligand (Fig. 7a, b). Both the PL spectra of $[Nd(Pic)_2(H_2O)_6](Pic)\cdot 6H_2O$ [28] and its complex were similiar, indicating that the acyclic ligand did not contribute to enhance the emission of the Nd complex. The $[Nd(Pic)(H_2O)_2(NO_3)(EO3)](Pic)$ complex showed broad bands at 403, 486, and 682 nm with the highest luminescent peak at 403 nm. Further, it did not display the 4f-4f transition. Formation of the specified peaks was attributed to the intraligand π–π transition of the Pic anion. In this complex, the resonance level of Nd(III) is below the triplet state of the HPic molecule; thus, the energy back transfer to the triplet state of the ligand dominates [30]. As previously reported, the emission characteristics of the Nd(III) ion at 1064, 890, and 1336 nm corresponding to the $^4F_{3/2} \rightarrow {}^4I_{11/2}$, $^4F_{3/2} \rightarrow {}^4I_{9/2}$ and $^4F_{3/2} \rightarrow {}^4I_{13/2}$ transitions were observed in neodymium oxide nanocrystal/titania/ormosil composite sol gel thin film [32].

As shown in Fig. 8, the $[Sm(Pic)(H_2O)_2(NO_3)(EO3)](Pic)\cdot H_2O$ complex exhibited the strong red emission peak at 616.7 nm, with a shoulder at 615.0 nm due to the $^4G_{5/2} \rightarrow {}^6H_{9/2}$ transition. The emission of the [Sm(Pic)

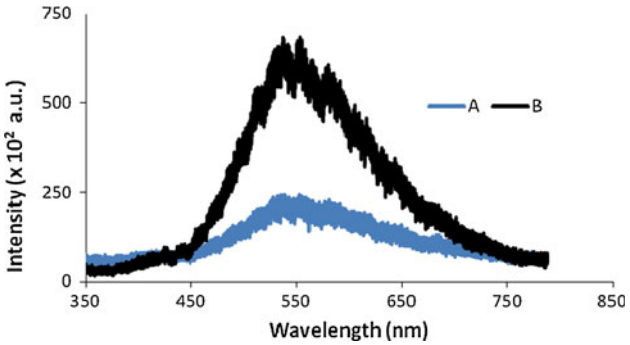

Fig. 6 Photoluminescence spectra of the HPic molecule (**a**) and $[Gd(Pic)_2(H_2O)(EO3)](Pic)\cdot CH_3OH$ complex (**b**) at room temperature with filter D2

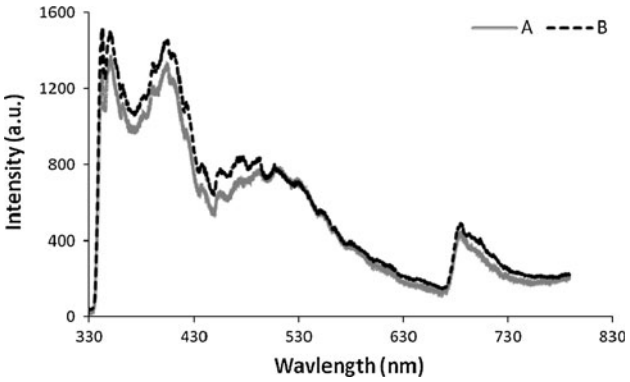

Fig. 7 Photoluminescence spectra of $[Nd(Pic)_2(H_2O)_6](Pic)\cdot 6H_2O$ (**a**) and $[Nd(Pic)(H_2O)_2(NO_3)(EO3)](Pic)$ (**b**) complexes at room temperature

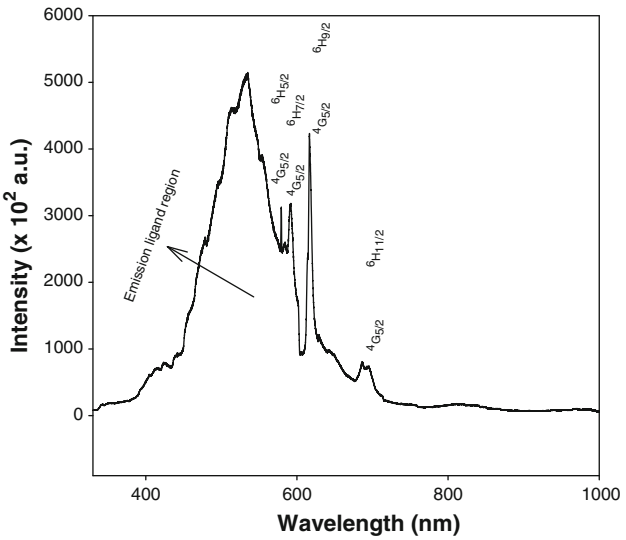

Fig. 8 The photoluminescent spectrum of the $[Sm(Pic)(H_2O)_2(NO_3)(EO3)](Pic)\cdot H_2O$ complex at room temperature

$(H_2O)_2(NO_3)(EO3)](Pic)\cdot H_2O$ complex exhibited not only the characteristic 4f-4f emission of Sm(III) ($^4G_{5/2} \rightarrow {}^6H_J$, J = 5/2, 7/2, 9/2, and 11/2), but also a stronger wide emission band (400–560 nm) for the HPic molecule. As shown in Table 4, the intensity ratio between the $^4G_{5/2} \rightarrow {}^6H_{9/2}$ transition allowed by the electric dipole and the $^4G_{5/2} \rightarrow {}^6H_{5/2}$ transition allowed by the magnetic dipole [I ($^4G_{5/2} \rightarrow {}^6H_{9/2}$) to I ($^4G_{5/2} \rightarrow {}^6H_5$)] was greater (1.36) in the Sm complex compared to Sm salt (1.32). Some internal energy levels, such as $^6F_{11/2}$; $^6F_{9/2}$; ^6H_J for J = 5/2, 7/2, 9/2; and 11/2, were present between the first excited state of $^4G_{5/2}$ and the ground state of $^6H_{9/2}$, giving rise to a non-radiative energy transfer process to lose the excited energy and reduce emission intensity [6, 30].

Table 4 Photoluminescent data for samarium nitrate salt and the Sm complex in solid state

Compound	λem (nm)	Intensity (a.u.)	Assignment
$[Sm(Pic)(H_2O)_2(NO_3)(EO3)](Pic)\cdot H_2O$	579.4	3091.4×10^2	$^4G_{5/2} \rightarrow {}^6H_{5/2}$
	584.9	2577.6×10^2	$^4G_{5/2} \rightarrow {}^6H_{7/2}$
	592.1	3176.1×10^2	
	615.0	2462.0×10^2	$^4G_{5/2} \rightarrow {}^6H_{9/2}$
	616.7	4199.6×10^2	
	687.2	803.2×10^2	$^4G_{5/2} \rightarrow {}^6H_{11/2}$
	695.9	688.9×10^2	
$Sm(NO_3)_3\cdot 6H_2O$	561.0	339.3	$^4G_{5/2} \rightarrow {}^6H_{5/2}$
	593.0	488.9	$^4G_{5/2} \rightarrow {}^6H_{7/2}$
	596.8	639.7	
	643.5	449.3	$^4G_{5/2} \rightarrow {}^6H_{9/2}$
	649.2	325.3	
	672.9	331.5	$^4G_{5/2} \rightarrow {}^6H_{11/2}$
	679.6	110.1	
	682.7	119.9	
	683.4	211.9	
	686.5	95.2	
	705.4	78.6	
	727.1	61.9	
	735.3	68.4	

Emission intensities of all 4f–4f transitions in the Sm complex were higher than those found in $Sm(NO_3)_3\cdot 6H_2O$. The broad peak related to the emission from the aromatic of the HPic ligand indicates that the Pic anion was inefficient at completely absorbing and transferring T_1(L) to the lowest excited resonance level of Sm(III) [31]. The PL spectrum of Sm salt, $[Sm(NO_3)_3.6H_2O]$, was observed and exhibited the emission typical for $^4G_{5/2} \rightarrow {}^6H_{11/2,\ 9/2,\ 7/2,\ 5/2}$ transitions (Table 4) [31]. In $Sm(NO_3)_3\cdot 6H_2O$, the hypersensitive electric dipole $^4G_{5/2} \rightarrow {}^6H_{7/2}$ transition was stronger than the magnetic dipole $^4G_{5/2} \rightarrow {}^6H_{9/2}$ transition [33]. In contrast with the $[Sm(Pic)(H_2O)_2(NO_3)(EO3)](Pic)\cdot H_2O$ complex, the $^4G_{5/2} \rightarrow {}^6H_{9/2}$ transition represented the strongest peak in the PL spectrum. In the Sm complex produced, the photoluminescent characteristics that showed emission characteristics of the Sm(III) ion

were clearly observed, unlike in the [Sm(Pic)$_2$(H$_2$O)(EO4)](Pic)·H$_2$O complex, where EO4 = tetraethylene glycol [31]. We assumed that the nitrate anion contributed to differences in crystal structure of the Sm(III) complex. We also observed that the NO_3^- anion is effective in chelation as a counter anion and does not quench energy transfer from the anion to the Sm(III) ion. In additon, the $^4G_{5/2} \rightarrow {}^6H_{9/2}$ transition exhibited a high level of sensitivity to relatively small changes in the chemical surroundings of the Sm(III) ion [6].

Conclusion

The isostructural [Nd(Pic)(H$_2$O)$_2$(NO$_3$)(EO3)](Pic) and [Sm(Pic)(H$_2$O)$_2$(NO$_3$)(EO3)](Pic)·H$_2$O complexes were synthesized and characterized. Both complexes showed a ten-coordination number. The nitrate anion was included in the inner-coordination sphere and replaced one picrate anion. The Ln-O_{EO3}, Ln–$O_{phenolic}$ and Ln-O_{nitro} bond lengths decreased with a decrease in the metal atom radius due to the lanthanide contraction effect. Several types of intra- and intermolecular O–H···O and C–H···O hydrogen bonds stabilized the crystal packing of the complexes. The photoluminescent spectrum of the Sm complex contains typical emissions of the $^4G_{5/2} \rightarrow {}^6H_{11/2,\ 9/2,\ 7/2,\ 5/2}$ transitions, with the strongest peak at 616.7 nm. Green emission from the Nd complex was attributed to the intraligand π–π transition of the Pic anion. We observed that the type, size, and shape of anions for charge balancing and stabilizing of the complex influenced the formation of the complex with either ten or nine coordinates. The series of ternary lanthanide-picrate-triethylene glycol complexes were investigated to evaluate the lanthanide contraction effect on structural properties.

Supplementary data

Crystallographic data for the structural analyses of the complexes were deposited with the Cambridge Crystallographic Data Center, CCDC 295233 [Nd(III) complex] and CCDC 667018 [Sm(III) complex]. Copies of this information may be obtained free of charge from: The Director, CCDC, 12 Union Road, Cambridge, CB2 1EZ, UK (Fax: +44-1223-336-033; e-mail: deposit@ccdc.cam.ac.uk or www: http://www.ccdc.cam.ac.uk).

Acknowledgments This study was supported by Universitas Indonesia (Hibah Kolaborasi Internasional Matching Fund 2012), and Universiti Sains Malaysia (USM RU Research Grant Number 1001/PKIMIA/811168).

References

1. Fan, Y., Yang, P., Huang, S., Jiang, J., Lian, H., Lin, J.: Luminescent and mesoporous europium-doped bioactive glasses (MBG) as a drug carrier. J. Phys. Chem. C **113**, 7826–7830 (2009)
2. Yang, P., Quan, Z., Li, C., Kang, X., Lian, H., Lin, J.: Bioactive, luminescent and mesoporous europium-doped hydroxyapatite as a drug carier. Biomaterials **29**, 4341–4347 (2008)
3. Panigrahi, B.S.: Synergistic fluorescence enhancement of Tb with aromatic monocarboxylic acids and TOPO–Triton X-100: role of Triton X-100 in synergism. Spectrochim. Acta A **56**, 1337–1344 (2000)
4. Bünzli, J.-G., Chauvin, A.S., Kim, H.K., Deiters, E., Eliseeva, S.V.: Lanthanide luminescence efficiency in eight- and nine-coordinate complexes: role of the radiative lifetime. Coord. Chem. Rev. **254**, 2623–2633 (2010)
5. Souza, A.P., Rodrigues, L.C.V., Brito, H.F., Alves Jr, S., Malta, O.L.: Novel europium and gadolinium complexes with methaneseleninate as ligand: synthesis, characterization and spectroscopic study. Inorg. Chem. Commun. **15**, 97–101 (2012)
6. Xu, C.: Luminescent and thermal properties of Sm^{3+} complex with salicylate and *o*-phenanthroline incorporated in silica matrix. J. Rare Earth **24**, 429–433 (2006)
7. Bünzli, J.-G., André, N., Elhabiri, M., Muller, G., Piguet, C.: Trivalent lanthanide ions: versatile coordination centers with unique spectroscopic and magnetic properties. J. Alloys Compd. **303–304**, 66–74 (2000)
8. Rogers, R.D., Zhang, J.: The effects of choice of anion (X = $C1^-$, SCN^-, NO_3^-) and polyethylene glycol (PEG) chain length on the local and supramolecular structures of LnX_3/PEG complexes. J. Alloys Compd. **249**, 41–48 (1997)
9. Rogers, R.D., Voss, E.J., Etzhenhouser, R.D.: Triethylene glycol complexes of the early lanthanide(III) chlorides. Inorg. Chim. Acta **196**, 73–79 (1992)
10. Rogers, R.D., Bauer, C.B.: In: Structural chemistry of metal-crown and polyethylene glycol complexes excluding groups 1 and 2. Dekalb, Northern Illinois University, Illinois (1996)
11. Saleh, M.I., Kusrini, E., Fun, H.K., Yamin, B.M.: Coordination of trivalent lanthanum with polyethylene glycol in the presence of picrate anion: spectroscopic and X-ray structural studies. J. Alloys Compd. **474**, 428–440 (2009)
12. Kusrini, E., Saleh, M.I.: Luminescence and structural studies of yttrium and heavier lanthanide–picrate complexes with pentaethylene glycol. Inorg. Chim. Acta **362**, 4025–4030 (2009)
13. Kusrini, E.: Triclinic structural and magnetic properties of praseodymium(III) picrate triethylene glycol complex. Inorg. Chim. Acta **363**, 2533–2538 (2010)
14. Kusrini, E., Saleh, M.I., Fun, H.K.: Triclinic structural isomer of cerium (III)-picrate complexes with triethylene glycol. J. Coord. Chem. **63**, 484–497 (2010)
15. Saleh, M.I., Kusrini, E., Mohd, Sarjidan, M.A., Abd. Majid, W.H.: Study and fabrication of europium picrate triethylene glycol complex. Spectrochim. Acta A **78**, 52–58 (2011)
16. Kusrini, E., Saleh, M.I., Yoshioka, N., Fun, H.K.: Crystal structure and photoluminescence properties of gadolinium picrate triethylene glycol complex. J. Chem. Crystallogr., Accepted (2012)
17. Kusrini, E., Saleh, M.I., Adnan, R.: Investigation of crystal structure influence on spectroscopic and photoluminescent properties of terbium picrate triethylene glycol complex. Spectrochim. Acta A, (2012)
18. Bruker, : APEX2, SAINT and SADABS. Bruker AXS Inc., Madison (2005)

19. Sheldrick, G.M.: Foundations of crystallography. Acta Crystallograph. A **64**, 112–122 (2008)
20. Spek, A.L.: Single-crystal structure validation with the program PLATON. J Appl. Cryst. **36**, 7–13 (2003)
21. Hirashima, Y., Tsutsui, T., Shiokawa, J.: X-ray structure analysis of neodymium nitrate complex with triethylene glycol. J Chem. Lett. 1405–1408 (1982)
22. Guo, Y.-L., Dou, W., Wang, Y.-W., Liu, W.-S., Wang, D.-Q.: Preparation, luminescent properties of *N*-phenyl-2-{2′-[(phenyl-ethyl-carbamoyl)-methoxy]-biphenyl-2-yloxy}-*N*-ethyl-acetamide (L) lanthanide complexes and the supramolecular structures of $[La(pic)_3L]$ and $2[La(NO_3)_3L(H_2O)]\cdot H_2O\cdot 0.5C_2H_5OH$. Polyhedron **26**, 1699–1710 (2007)
23. Carnall, W., Siegel, S., Ferrano, J., Tani, B., Gebert, E.: New series of anhydrous double nitrate salts of the lanthanides. Structural and spectral characterization. Inorg. Chem. **12**, 560–564 (1973)
24. Nakamoto, K.: Infrared and Raman spectra of inorganic and coordination compounds, 3rd edn. Willey, New York (1978)
25. Tai, X.-S., Tan, M.-Y.: Studies on synthesis, infrared and fluorescence spectra of new europium (III) and terbium (III) complexes with an β-diketonate-type ligand. Spectrochim. Acta A **61**, 1767–1770 (2005)
26. Forsellini, E., Casellato, U., Tomat, G., Graziani, R., Di Bernardo, P.: Trinitrato-(O, O')(triethylene glycol)europium(III), Eu(NO3)3(C6H14O4). Acta Crystalogr. C **40**, 795–797 (1984)
27. Nealon, G.L., Mocerino, M., Ogden, M.I., Skelton, B.W.: The impact of the lanthanide contraction on the structure of complexes of a calix[4]arene trisamide. J. Incl. Phenom. Macrocycl. Chem. **65**, 25–30 (2009)
28. Saleh, M.I., Kusrini, E., Fun, H.K., Yamin, B.M.: Structural and selectivity of 18-crown-6 ligand in lanthanide-picrate complexes. J. Organomet. Chem. **693**, 2561–2571 (2008)
29. Shannon, R.D.: Revised effective ionic radii and systematic studies of interatomic distances in halides and chalcogenides. Acta Crystallogr. A **32**, 751–767 (1976)
30. Xu, C.: Photophysical properties of lanthanide complexes with 5-nitro-1,10-phenanthroline. Monatsh. Chem. **141**, 631–635 (2010)
31. Kusrini, E., Saleh, M.I., Yulizar, Y., Za'aba, N.K., Abd. Majid, W.H.: Samarium(III) picrate tetraethylene glycol complex: Photoluminescence study and active material in monolayer electroluminescent. J. Lumin. **131**, 1959–1965 (2011)
32. Que, W.X., Zhou, Y., Lam, Y.L., Kam, C.H., Zhou, J., Pita, K., Chan, Y.C., Buddhudu, S., Gan, L.H., Deen, G.R.: Photoluminescence characteristics of neodymium oxide nanocrystal/titania/ormosil composite sol-gel thin films. Appl. Phys. A **73**, 485–488 (2001)
33. Kiisk, V., Sildos, I., Lange, S., Reedo, V., Tätte, T., Kirm, M., Aarik, J.: Photoluminescence characterization of pure and Sm^{3+}-doped thin metal oxide films. Appl. Surf. Sci. **247**, 412–417 (2005)